Technical Report: RL-1006

DESIGN OF AN ULTRA-FAST WIDE-BAND MMW POLARIMETRIC INSTRUMENTATION RADAR

Adib Y. Nashashibi

Kamal Sarabandi

Panayiotis Frantzis

Roger D. De Roo

Fawwaz T. Ulaby

Contract #: QK 8820

June 2002

The Radiation Laboratory

Department of Electrical Engineering and Computer Science

The University of Michigan, Ann Arbor, MI 48109-2122

RL-1006 = RL-1006

Abstract

With the advent of high frequency RF circuits and components technology, millimeter-wave (MMW) radars are being proposed for a large number of military and civilian applications. Accurate and high resolution characterization of the polarimetric radar backscatter responses of both clutter and man-made targets at MMW frequencies is essential for the development of radar systems and optimal detection and tracking algorithms. Towards this end, a new design is developed for ultra-fast, wide-band, polarimetric, instrumentation radars that operate at 35 and 95 GHz. With this new design, the complete scattering matrix of a target (magnitude and phase) can be measured over a bandwidth of 500 MHz in less than 2 μsec. In this paper, the design concepts and procedures for the construction and calibration of these radars are described. In addition, the signal processing algorithm and data-acquisition procedure used with the new radars are presented. To demonstrate the accuracy and applicability of the new radars, backscatter measurements of certain point and distributed targets are compared with their analytical RCS and previously measured σ^o values, respectively, and good agreements are shown. These systems, which can be mounted on a precision gimbal assembly that facilitates their application as high resolution imaging radar systems, are used to determine the MMW two-way propagation loss of a corn field for different plant moisture conditions.

*Prepared through collaborative participation in the Advanced Sensors Consortium sponsored by the U.S. Army Research Laboratory under the Federated Laboratory Program, Cooperative Agreement DAAL01-96-2-0001.

Contents

1 INTRODUCTION **1**

2 SYSTEM DESCRIPTION **4**

2.1 The Linearly-Chirped Pulse Generator Module 5

2.2 The RF Frontend Module 7

2.3 The Receiver Module 8

2.4 Control Circuit 9

3 MEASUREMENT AND SIGNAL PROCESSING PROCEDURES **11**

3.1 Signal Processing 12

4 SYSTEM CALIBRATION AND VALIDATION **18**

5 EXAMPLE OF REMOTE SENSING STUDIES OF TERRAIN **20**

6 CONCLUSIONS **24**

List of Figures

1 System block diagram of the new radar design. 4

2 Block diagram of the linear-chirp pulse generator module. 6

3 Spectral purity of the chirped-pulse generation module. To demonstrate the spectral purity of the chirped pulse generation circuit, a CW signal was generated instead of the chirped pulse. Spurious signals are at least 60 dB below the transmitted signal and are 10 MHz apart. This frequency separation is consistent with the frequency of the internal crystal driving the 500-MHz clock. 7

4 Block diagram of the 95-GHz RF frontend module. 8

5 Block diagram of the receiver module. 9

6 Block diagram of the programmable pulse delay and control circuit. 10

7 The measured system responses due to backscatter by a metallic sphere, when processed according to the expressions in (1) and in (2). The dashed line refers to (1) while the solid line refers to (2). 14

8 A flow chart demonstrating the procedure that was used to process the acquired data. 15

9 Comparison between the radar return due to a single pulse (solid line) and the result of coherently subtracting the radar returns of two consecutive pulses (dotted line). 16

10 Comparison between the response of a single pulse and the coherently averaged response of 16 pulses. Coherent averaging provides about 6 dB improvement in the target signal-to-mean noise floor ratio. 17

11 The magnitude (a) and phase difference (b) of the scattering matrix elements of a metallic cylinder (3.665 cm in length and 0.23 cm in diameter) oriented at 43^o from vertical. 20

12 The backscattering coefficients of a dry smooth asphalt surface measured once in 1996 using a network analyzer-based scatterometer operating at 95 GHz, and measured one more time in 1998 using the new ultra-fast wide-band scatterometers at 35 GHz and 95 GHz. The rms height and correlation length of the asphalt surface were 0.34 mm and 4.2 mm respectively. 21

13 A vv-polarized near-grazing radar image of a corn field measured at 35 GHz. The normalized received power is plotted versus range in meter. 22

14 The average time-domain return from dry corn at 95 GHz. 23

15 Two-way propagation loss per row in a corn field during its life cycle measured at both 35 and 95 GHz, as a function of, m_g, the average gravimetric moisture content in the plants. Increased plant moisture is correlated with increased propagation loss. 23

1. INTRODUCTION

With the recent advancements in semiconductor technology, reliable and relatively inexpensive millimeter-wave (MMW) radars are now attainable. Due to the inherent advantages of MMW radars over other sensors, namely their compactness, high resolution, and near all-weather capabilities, they have been proposed for a number of applications, including vehicle collision avoidance, traction control, robotics, and autonomous vehicle control. In most applications, the success of MMW radars is measured by their ability to detect targets in the presence of clutter or by their ability to measure certain properties of a target with an acceptable accuracy. The design of the optimum radar system and the development of the best target-detection algorithm for a particular application require an accurate a priori knowledge of the polarimetric radar backscatter responses of clutter and of the targets of interest. Proper characterization of the backscatter responses of both clutter and man-made targets is best achieved through the use of polarimetric instrumentation radars capable of characterizing the backscattered field by measuring its polarization, magnitude, and phase, accurately.

Three critical attributes are desired in a MMW instrumentation radar to ensure its versatility: full polarimetry, high resolution imaging capability, and fast data acquisition. A fully polarimetric radar allows for the measurement of the complex elements of the scattering matrix of a target in a given orthogonal polarization basis (such as the vertical, V, and horizontal, H, polarization basis), from which the radar response in any other transmit/receive polarization configuration can be synthesized [1,2]. In phenomenological studies of radar backscatter, high-resolution radar imaging (both in range and along track) can provide insight to the sources responsible for the different scattering mechanisms contributing to the overall backscatter from a given clutter type or man-made target. The high resolution capabilities can also be used to study the properties of signals propagating through turbulent media such as foliage and rain. It can also form the basis for evaluating the performance of optimal detection and tracking algorithms. While along-track spatial resolution can be achieved through the use of an electrically large aperture, range resolution can only be achieved through the use of a narrow pulse, or equivalently a wide bandwidth. At millimeter-wave frequencies, at least 500 MHz of signal bandwidth, which

corresponds to one-foot range resolution, is required for certain applications and phenomenological studies. It should be noted that the polarimetric measurements need to be performed over the entire signal bandwidth if high-resolution polarimetric images are to be generated. Since the phase of the backscattered signal must be preserved, it is required that the measurement of the scattering matrix elements be completed, over the entire bandwidth, within a period of time sufficiently short to ensure that signal correlation between the scattering matrix elements is maintained. Temporal decorrelation is often due to the relative movement of target or clutter (such as foliage) elements with respect to the radar platform. For example, at 95 GHz (wavelength $\lambda = 3.2$ mm) a 25^o phase error is introduced over 20 μsec for an object moving at a low speed of 20 km/hr.

Vector network analyzer-based instrumentation radars [2, 3] operating in a stepped frequency continuous-wave mode have been used in the past for characterizing the clutter response at both microwave and millimeter-wave frequencies. Although these radars can measure the magnitude and phase of the radar signal over a wide frequency range and with high precision and accuracy, the long data-acquisition time required for these systems (0.5 second per transmitted polarization) renders them less attractive for outdoor, polarimetric measurements at MMW frequencies, especially when foliage is the target to measure. Although Frequency Modulated Continuous Wave (FMCW) radars have been proposed for certain applications at MMW frequencies, the difficulty in extracting the phase of the backscattered signal and the linearity constraints on the frequency chirp over the entire band make them less attractive for use as instrumentation radars. Pulse-based polarimetric instrumentation radars have been also used at MMW frequencies [4]. They transmit high-peak power pulses at a single carrier frequency (with the receiver switched off during transmission) and they use I-Q channels for the detection of the magnitude and phase of the received signal. A major limitation of pulsed MMW systems is that they have coarse range resolution because generating pulses on the order of nanoseconds in length is both difficult and expensive. To improve the range-resolution capability of a pulse radar, the carrier frequency can be stepped over a certain bandwidth [5] and then through proper signal processing of the received series of pulses, significant improvement in range-resolution can be achieved. However, the time needed to acquire data for generating the scattering matrix with the desired resolution is rather long and is limited by the pulse repetition rate of the system.

The FM chirped pulse radar, which combines the advantages of FMCW radars (wide-band and low peak power) and pulse radars (fast data acquisition and phase-angle measurements), have also been used in many applications [2]. However, linearity constraints on the FM chirp over the desired signal bandwidth and the limited bandwidth of the Surface Acoustic Wave devices (SAW) often used in these systems, have prohibited their use at MMW frequencies. With recent advances in computer technology and high-speed samplers and A/D converters, FM chirped pulse-based instrumentation radars are now feasible at MMW frequencies. The SAW and I-Q channels constituting the conventional receiver in FM chirped pulse radars can be replaced with a digitizing oscilloscope. Modern digitizing oscilloscopes use special techniques to combine a set of fast samplers together in order to achieve sampling rates as high as 2 Giga samples/sec so as to sample, in real time, signals up to 1 GHz in frequency. In addition, the development of direct digital synthesizers and chirp generators employing fast D/A converters have permitted the generation of highly linear FM-CW waveforms. Through proper frequency multiplication and up-conversion schemes, a rather wide-band, highly linear, FM-chirped pulses can be generated at MMW frequencies as will be described in this paper.

This paper describes a new design of an instrumentation radar, based on the FM chirped-pulse approach, that overcomes the inherent speed limitations of stepped frequency radars and permits wide-band polarimetric backscatter measurements to be conducted in less than 2 μsec. In this novel and relatively inexpensive design, an ultra-fast synthesizer (2 nsec/step) is used as the linear chirp generator and a real-time ultra-fast multi-channel digitizing oscilloscope (2 Giga Samples/sec) is used as the IF detector. Using appropriate multiplier, filter, and amplifier combinations, a chirp bandwidth of up to 840 MHz is generated (with controllable pulse width of 0.5-16 μsec) which is then up-converted to the desired RF frequency before transmission. The system has the ability to collect internally a sample of each transmitted pulse. This "reference" signal permits continuous monitoring of the system transfer function and is used in subsequent signal-processing to enhance signal quality. Using narrow beam antennas, high resolution images can be easily generated using this system. In addition, with proper signal processing, the response from a particular target can be isolated (through the application of software gating) and its frequency response can be characterized.

The paper demonstrates also the high resolution imaging capabilities of the new system. The sensitivity of the radar return to the periodic row stracture of a corn field, imaged at 35-GHz and 95-GHz, is demonstrated. In addition, the two-way propagation loss inside the corn field is derived from the images for different plant moisture conditions.

In the next section, a detailed description is provided of the new ultra-fast, wide-band (high resolution), instrumentation radar structure. The associated signal processing technique and measurement procedure are described in Section 3, and in Section 4, system calibration and validation are addressed. Examples demonstrating the imaging capabilities of the system are presented in Section 5.

2. SYSTEM DESCRIPTION

At millimeter-wave frequencies, it is difficult to generate and detect a wide-band linearly-chirped pulse directly. Instead, chirp pulse generation and detection must be conducted at an intermediate frequency (IF). In this case, the MMW components of the radar are restricted to up- and down-conversion of the IF chirped pulse to MMW chirped pulses which in turn are transmitted/received *via* an antenna assembly. The ultra-fast, wide-band system, depicted in Fig. 1, consists of three main modules: (1) the linearly-chirped pulse generator module, (2) the MMW RF frontend module, and (3) the receiver module. The system as it stands is modular, compact, light weight, relatively inexpensive, and can be mounted on a gimbal inside a van (for near grazing imaging applications) or atop a boom truck.

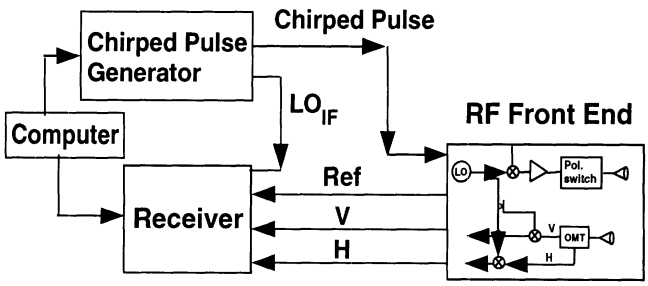

Figure 1: System block diagram of the new radar design.

2.1. The Linearly-Chirped Pulse Generator Module

The linearly-chirped pulse generator module is designed around a direct digital chirp synthesizer (DCP) unit [6]. The DCP unit consists of the more traditional direct digital synthesizer with a frequency accumulator added in front of the phase accumulator to provide the unit with linear-sweep capability. The computer-controlled DCP unit can be configured so as to generate a pulse whose frequency is chirped between two frequencies, a start frequency f_{start} and a stop frequency f_{stop}, spanning anywhere between 1 MHz and 230 MHz. The chirping is accomplished by stepping in frequency at equal increments Δf (minimum step size is 29.8 Hz) every 2 nanoseconds. Both chirp bandwidth and pulsewidth can be controlled *via* a computer through the proper choice of the programmable f_{start}, f_{stop}, and Δf frequencies. In addition, the unit can be operated in a CW mode by setting Δf to zero. The direct digital chirp synthesizer unit requires a 500 MHz reference clock (2 nanosecond period) which is provided through a separate 10 MHz crystal-referenced synthesized source.

A linearly-chirped pulse, generated using the DCP unit, can span at most a bandwidth of 230 MHz, which might not be sufficient for certain high resolution MMW radar applications where at least 500 MHz bandwidth is needed. In addition, it is difficult to up-convert a baseband signal, such as that generated by the DCP unit, directly to MMW frequencies (the lower and upper images after up-conversion to MMW frequencies are, in this case, too close to each other and cannot be isolated efficiently). To overcome these two limitations, a special frequency multiplication circuit, shown in Fig. 2, was designed and constructed for the dual purpose of expanding the chirp bandwidth and translating the chirp from baseband to an intermediate frequency (C-band in this case) amenable for subsequent up-conversion to MMW frequencies. The circuit also utilized the available 500 MHz clock signal to generate a coherent CW signal at C-band to be used in the receiver module for down-converting the backscattered chirped pulse to baseband (where detection can be easily accomplished).

In Fig. 2, the 500-MHz clock is the common source for the entire module, thereby ensuring signal coherence. A chirped pulse spanning between 125 and 230 MHz is translated in frequency to 625-730 MHz chirp by mixing it with the 500 MHz reference clock. Then, through a set of properly designed filters, amplifiers, and frequency

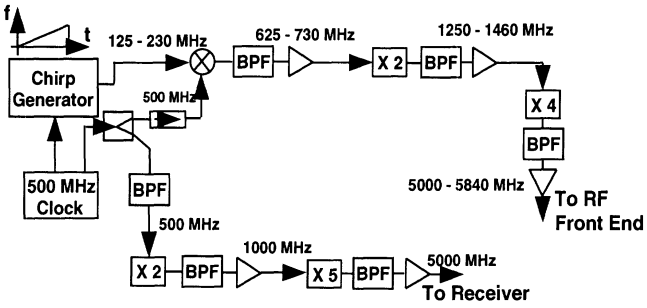

Figure 2: Block diagram of the linear-chirp pulse generator module.

multipliers, a chirped pulse from 5.0 to 5.84 GHz is generated. Similarly, a 5.0-GHz reference CW signal is generated from the 500-MHz clock using the $\times 10$ frequency multiplier circuit shown in Fig. 2. Chirp bandwidth less than 840 MHz can be easily achieved by lowering the stop frequency in the DCP unit to less than 230 MHz without altering the circuit in Fig. 2.

The chirp start frequency of 125 MHz was chosen for a number of reasons: (1) to ensure that high-order harmonics of the original chirped pulse (125-230 MHz) are outside the chirp bandwidth, and therefore they can be easily filtered out, (2) by translating the chirp to start at 625 MHz, a bandpass filter can be easily designed to suppress both the original chirped pulse (125-230 MHz) and the 500 MHz signal leaking through the up-converter, and (3) the $\times 8$ multiplication of 625 MHz results in a 5000 MHz signal which is at the same frequency as the CW reference signal to be used by the receiver module. All filters used in the frequency multiplication circuit were designed so as to filter out undesirable harmonics of the chirped pulse generated during the frequency multiplication process. In addition, special care was taken to ensure high isolation between the chirp-pulse generation section and the reference-signal section (through the use of an isolator and a narrow bandpass filter just after the power divider of the 500 MHz signal, as shown in Fig. 2).

The linearly-chirped pulse generator module was constructed and tested for spectral purity. Over the entire bandwidth of interest, spurious signals and higher order harmonics were at least 60 dB below the carrier, as illustrated in Fig. 3.

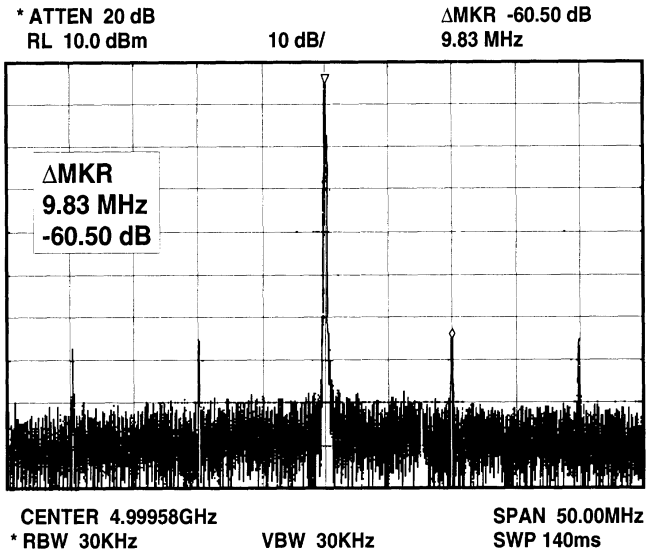

Figure 3: Spectral purity of the chirped-pulse generation module. To demonstrate the spectral purity of the chirped pulse generation circuit, a CW signal was generated instead of the chirped pulse. Spurious signals are at least 60 dB below the transmitted signal and are 10 MHz apart. This frequency separation is consistent with the frequency of the internal crystal driving the 500-MHz clock.

2.2. The RF Frontend Module

The primary function of the RF frontend module is to: (a) up-convert an IF chirped pulse (5.0-5.84 GHz) to MMW frequencies, (b) transmit the MMW chirped pulse at a given polarization (V or H), and (c) receive the orthogonal components (V and H) of the backscatter target response and down-convert them to IF frequencies for subsequent detection. A block diagram of the University of Michigan's 95-GHz RF frontend module is shown in Fig. 4. In this module, a dual-antenna system (transmit and receive antennas with 2.8^o and 1.4^o beamwidths, respectively) operating in monostatic mode was used. The transmit antenna is fed by an orthomode transducer and a high-isolation (40-dB) high-speed (20 nanosecond) SPDT switch intended for transmit polarization selection. The receive antenna is a Gaussian optics antenna (high efficiency and low sidelobe levels) with an internally installed wire grid polarizer of 40-dB polarization isolation. The wire grid decomposes the received response into its V and H orthogonal components. A single 89.5-GHz local oscillator was used to provide the necessary LO power for both up- and down-conversion, hence maintaining signal coherence in the system. Both

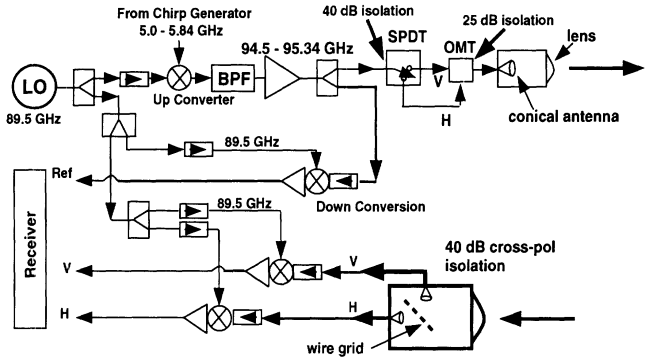

Figure 4: Block diagram of the 95-GHz RF frontend module.

V and H components of the backscattered response are down-converted simultaneously along with a sample of the transmitted pulse (*Ref*) as shown in Fig. 4. As mentioned before, the *Ref* channel plays an important role in signal processing of the backscattered response as will be demonstrated in Section 3. A similar module was constructed at 35 GHz (with LO at 29.8 GHz).

2.3. The Receiver Module

The receiver module, shown in Fig. 5, consists of three C-band mixers followed by baseband amplifiers (0-1000 MHz), which in turn feed a four-channel wide-band Digitizing Oscilloscope (DO). The 5.0-5.84 GHz signals of the V, H, and *Ref* channels of the RF frontend are down-converted to baseband (0-840 MHz) using the 5.0-GHz reference signal provided by the linearly-chirped pulse generator module. The baseband signals are then amplified before being digitized (i.e., sampled and A/D converted) in real time at a rate higher than the Nyquist frequency.

At The University of Michigan, an HP54542C Digitizing Oscilloscope (manufactured by Hewlett Packard Co.) is used for sampling and digitizing. It has four parallel channels capable of digitizing signals at a maximum real-time rate of 2 Giga samples/sec/channel. It can detect signals with frequency contents between 0 and 500 MHz in real time and possesses a 50-dB dynamic range with 40-dB channel to channel isolation. In addition, it can store internally up to 32K samples/channel (equivalent to 16 μsecond worth of data sampled at 2 Giga samples/sec.).

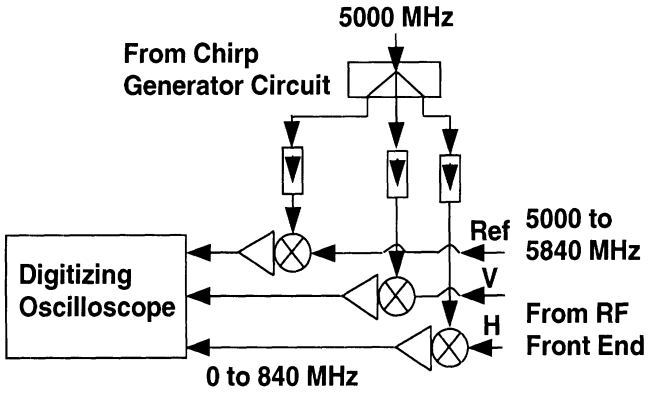

Figure 5: Block diagram of the receiver module.

Three of the four DO channels are used for detecting the V, H, and *Ref* signals while the fourth channel is connected directly to the DCP chirp *enable* pin and is used as a trigger for DO. Although the new radar system can generate and transmit a chirped pulse of bandwidth up to 840 MHz, the receiver is band-limited by the present DO to 500 MHz only.

2.4. Control Circuit

During a given data-acquisition exercise (in which the DO will digitize continuously until the allocated memory storage is full) the radar system will cycle between three basic steps: (1) generate and transmit a linearly-chirped pulse, (2) digitize the received radar backscatter response, and (3) switch to the other transmitted polarization between consecutive pulses. It should be noted that the "listen" time between successive pulses, where no signals are transmitted, should be proportional to the round trip time necessary for the latest part of the chirped pulse to return from the farthest target of interest. Since the DCP unit does not have the capability to switch off on its own for a prescribed time proportional to the desired "listen" time before re-transmitting once again, a programmable pulse delay and control circuit was designed and built for this task.

The control circuit, shown in Fig. 6, synchronizes the tasks of the three modules comprising the radar system. Its function is to use the inverted TTL pulse (a 28 nanosecond pulse generated at the end of a chirp) from the output port S2 of the DCP unit to disable pulse generation in the DCP momentarily. The same inverted TTL pulse is

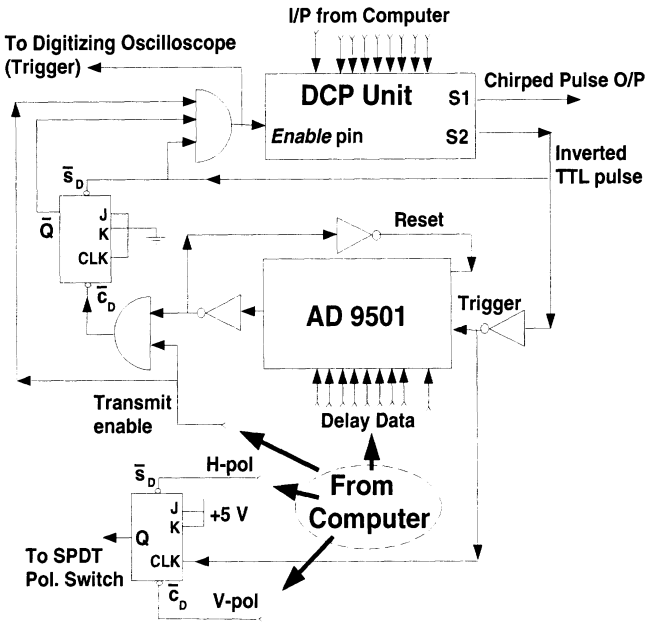

Figure 6: Block diagram of the programmable pulse delay and control circuit.

also used to trigger a digitally programmable delay generator chip (in this paper, the AD9501 chip manufactured by Analog Devices was used) which in turn generates a pulse at the end of a prescribed delay period (can be made equal to the "listen" time) to *enable* the DCP unit and start the chirp pulse generation once again. The control circuit has the capability of switching the transmit polarization state during the delay period also.

The computer can stop the chirping process at any time *via* the control circuit. Also, it has the option of either alternating the transmit polarization state between successive pulses or limiting transmission to one polarization state only. However, since computer speeds and software efficiencies vary, the computer in this system is expected to serve the following functions: (1) load the DCP unit with the desired values for f_{start}, f_{stop}, and $\Delta\ f$, (2) load the programmable delay generator chip (shown in Fig. 6) with the desired delay time value, (3) configure the DO (initialize, load the desired sampling rate, activate all four channels, etc.) and arm it (set it to proper trigger mode), (4) switch the SPDT switch in the RF frontend to the desired start polarization, (5) initiate data acquisition, and (6) unload data off of the DO storage memory at the end of data acquisition and process and store the data.

A radar system with the aforementioned architecture offers a number of advantages besides the high speed data

collection capability. For example, since the transmitted pulse is chirped, the desired range resolution is achieved irrespective of the actual pulsewidth used. Hence, a pulse that is several microseconds long can be transmitted. A microsecond pulse length yields two advantages over a nanosecond pulse: a lower peak transmit power and an improved signal-to-noise ratio in the received signal. This is particularly advantageous at millimeter-wave frequencies where millimeter-wave tubes can be replaced with solid-state power amplifiers. In addition, if the pulse peak power was low enough such that the receiver part of the RF frontend need not be switched off during pulse transmission, then RF switches (normally present in the receiver of high power pulse systems) can be excluded from the design, thereby improving the receiver's noise figure. Furthermore, measurements of targets located in the vicinity of the radar (i.e., at ranges shorter than the pulsewidth) can be conducted.

It should be noted that the system design described above is not restricted to MMW radars. In fact, ultra-fast, wide-band, polarimetric instrumentation radars operating at any frequency band can be constructed easily using the present design. This can be achieved by simply replacing the 95-GHz RF frontend with other frontends while retaining the chirped pulse generator module, the receiver module, and the control circuit. Both 35 and 95-GHz frontends were used together in recent outdoor measurements. Four IF SPDT computer-controlled switches were used to alternate between the IF ports of the 35 and 95-GHz frontends as the two frontends were imaging a distributed target.

3. MEASUREMENT AND SIGNAL PROCESSING PROCEDURES

The measurement procedure can be summarized as follows: first, the start, stop, and increment step frequencies of the DCP unit are set. Then, the switch-off time of the pulse delay circuitry is set based on the maximum range of interest, the SPDT transmit polarization switch is set to V polarization, and the DO is armed. Once the measurement process is initiated by the computer, the chirp generator is switched-on, the Digitizing Oscilloscope is triggered to sample signals from the V, H, and *Ref* channels. At the end of the chirp, the chirp generator is automatically switched-off for the prescribed "listen" time, the polarization switch is switched to the other

polarization while the DO continues to sample the received signals. The chirp is then activated again and the process continues automatically until the DO data storage memory is full. At this time, the computer stops the chirp, resets the polarization switch, transfers the sampled data from the DO data bank, and processes the data. Depending on the pulse length and the switch-off time selected, anywhere from one to several pairs of transmitted pulses can be measured (corresponding to one or several scattering matrices for each target present in the signal propagation path).

3.1. Signal Processing

As mentioned before, long pulses with wide-band chirps are employed in the proposed radar design. Whether the targets are close or far away from the radar, the radar return at any instant of time will be a superposition of fields scattered from targets that are located at different ranges and illuminated by different portions of the transmitted pulse (i.e., at different frequencies). Nevertheless, at the end of the DO operation, each target would have been illuminated by the entire transmitted pulse and its backscatter response would have been detected. In effect, the information about the scattering properties of a given target and its location in range are distributed over the entire received return. Further processing of the sampled data is needed.

Let the output of the reference channel be denoted by $R_{ref}(t)$. Similarly, let the outputs of the V- and H-receiver channels be denoted by $R_{ij}(t)$ (where i refers to the received v- or h-polarized channels and j refers to the transmitted v or h polarization). The standard approach in processing the radar return (due to a chirped pulse) is to pass it through a filter, $h(t)$, whose bandwidth is equal to the inverse of the pulse duration [7]. Mathematically, the output of the filter, $s_{ij}(t)$, is the result of a convolution process between the signal and the filter, $s_{ij}(t) = R_{ij}(t) * h(t)$, in the time domain. In the frequency domain, the output can be expressed as the multiplication of the frequency response of the signal with that of the filter, $S_{ij}(f) = \tilde{R}_{ij}(f).H(f)$. It can be shown that a maximum signal-to-noise ratio (SNR) can be achieved when the filter is proportional to the complex-conjugate of the signal itself, $H(f) = K\tilde{R}^{*}_{ij}(f)$, where K is a constant [7]. The filter in this case is called a "matched" filter. It should be noted that inherent in the assumptions leading to the derivation of the

matched filter (with maximum SNR) is that the radar system is ideal.

As mentioned before, the signal in the reference channel is a faithful representation of the transmitted pulse. Hence, $\tilde{R}^*_{ref}(f)$ can be used as the matched filter in computing $S_{ij}(f)$

$$S_{ij}(f) = \tilde{R}_{ij}(f).\tilde{R}^*_{ref}(f) \tag{1}$$

The measured radar return from a metallic sphere was processed using (1) and its inverse fast Fourier transform (IFFT) is plotted in Fig. 7 (dashed line). It is observed that applying the matched filter directly has resulted in a higher noise floor and higher sidelobe levels than expected. This can be attributed to the fact that the magnitudes of both $\tilde{R}_{vv}(f)$ and $\tilde{R}^*_{ref}(f)$ are not constant; instead, they are functions of frequency. To alleviate this problem a special window function needs to be designed and implemented. Of course, the inclusion of a window function will inevitably result in a modified matched filter, $H(f) = \tilde{R}^*_{ref}(f).W(f)$, that does not necessarily provide the optimum SNR. A radar system typically contains several time-variant devices, such as amplifiers and mixers, hence, the window function must be updated periodically to account for temporal variations in the transfer function of the system.

In this paper, we propose an alternative approach, namely that $S_{ij}(f)$ is computed using the reference division, as given by following expression

$$S_{ij}(f) = \frac{\tilde{R}_{ij}(f)}{\tilde{R}_{ref}(f)} \tag{2}$$

applied only over f within the desired bandwidth, otherwise $S_{ij}(f) = 0$. In other words, the matched filter is replaced with $1/\tilde{R}_{ref}(f)$. In this approach, the phase-conjugation of the signal, which is necessary for proper focusing of different target returns, is achieved while the magnitude variations over frequency are corrected at the same time. As a result, an improved time-domain response is obtained (see the solid line in Fig. 7). In addition, any temporal variations in the transmitted pulse will be corrected for instantaneously.

A flow chart that demonstrates the signal processing procedure being proposed for processing the data is shown in Fig. 8. In this procedure, the fast Fourier transform (FFT) is applied to the sampled data first. Then, the

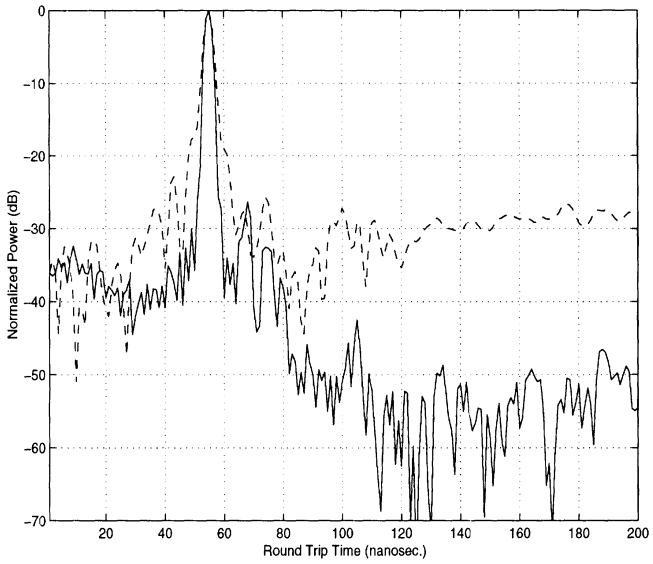

Figure 7: The measured system responses due to backscatter by a metallic sphere, when processed according to the expressions in (1) and in (2). The dashed line refers to (1) while the solid line refers to (2).

resulting frequency responses of the V- and H-receiver channels are computed using the expression in (2) at every point within the measured bandwidth. If desired, the $S_{ij}(f)$ can be calibrated against the measured frequency response of a calibration target (metallic sphere or trihedral). In addition, a high resolution time domain response of a distributed target illuminated by the radar antenna can be obtained by first multiplying $S_{ij}(f)$ with an appropriate window function (to suppress sidelobes), then, performing an IFFT on the product.

In cases where the frequency response of a particular target within the radar beam needs to be isolated from that of other targets, software gating on the target's time-domain response should be performed first. Then, the frequency response of the target can be retrieved from the gated response through an additional FFT step.

The new system is stable enough so that signal coherence between consecutive transmitted pulses is maintained. This is critically important for both the scattering matrix measurement and for cases where coherent subtraction and/or coherent averaging of the radar returns are needed. Coherent subtraction is often needed in situations where the response of an unwanted background perturbs that of a desired target. In this case, the background is measured first, then, its frequency response is coherently subtracted from the response of the target+background case. In Fig. 9, the time-domain response of two point targets due to a single pulse (solid line) is compared to

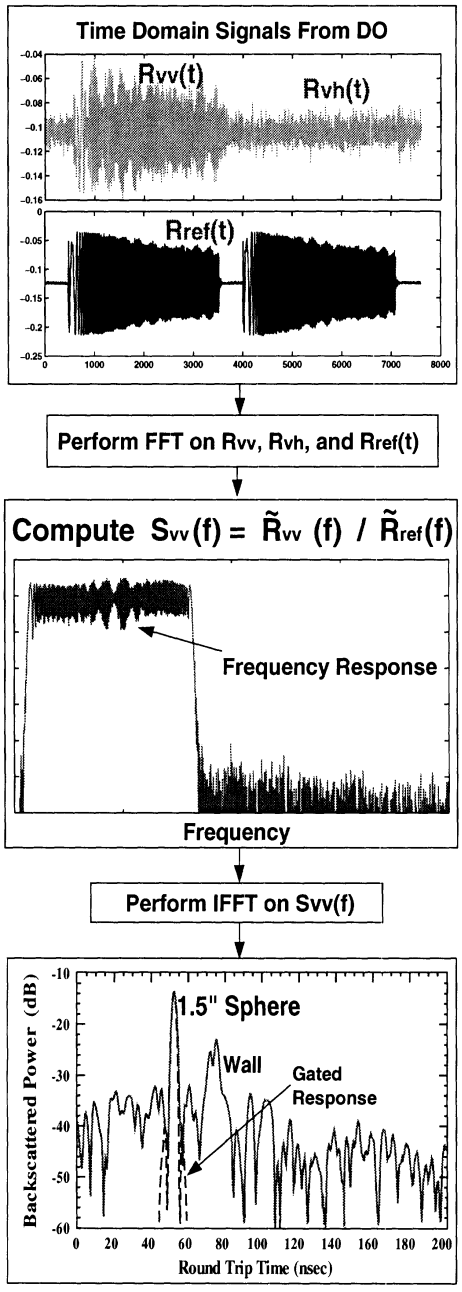

Figure 8: A flow chart demonstrating the procedure that was used to process the acquired data.

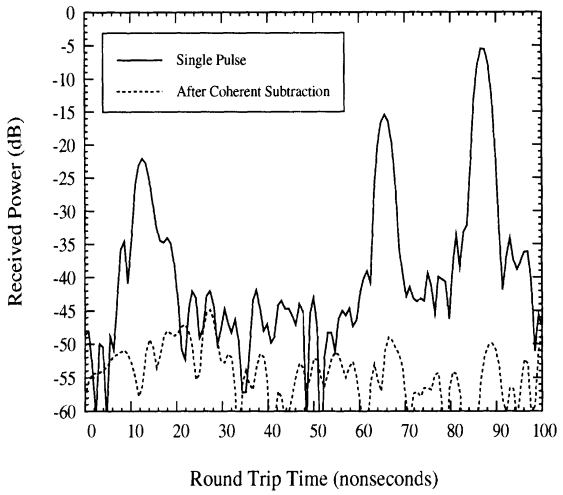

Figure 9: Comparison between the radar return due to a single pulse (solid line) and the result of coherently subtracting the radar returns of two consecutive pulses (dotted line).

the coherently subtracted responses of the same targets due to two consecutively transmitted pulses (dotted line). It should be noted that the residue from the coherent subtraction in this case is 50 dB lower than the strongest target return and is limited by the DO dynamic range (50 dB). Additional tests of the new system have yielded the same level of signal coherence for periods exceeding 1 hour in an indoor setting (i.e., at a fixed ambient temperature).

In cases where weak target returns are observed, coherent averaging of sequentially transmitted pulses can be applied to improve the SNR by reducing the effects of the system's noise. Consider the case where N pulses are sequentially transmitted (of course, they are interleaved with the proper "listen" time). The sampled return at each of the DO channels can be dissected into N returns, each corresponding to one of the pulses that were transmitted. Two averaging schemes were investigated for the proposed system: the first involves averaging the $R_{vj}(t)$, $R_{hj}(t)$, and $R_{ref}(t)$ of the dissected pieces (averaging real numbers). The averaged samples $< R_{vj}(t) >$, $< R_{hj}(t) >$, and $< R_{ref}(t) >$ (where $<>$ refers to the ensemble average) are then used in (2) to compute the frequency response of the target. In the second averaging scheme, the frequency response of the target $S_{ij}(f)$ is computed first for each pulse using the expression in (2). Then the resulting complex frequency responses are averaged coherently to produce $< S_{ij}(f) >$. The two approaches were tested against the measured response of

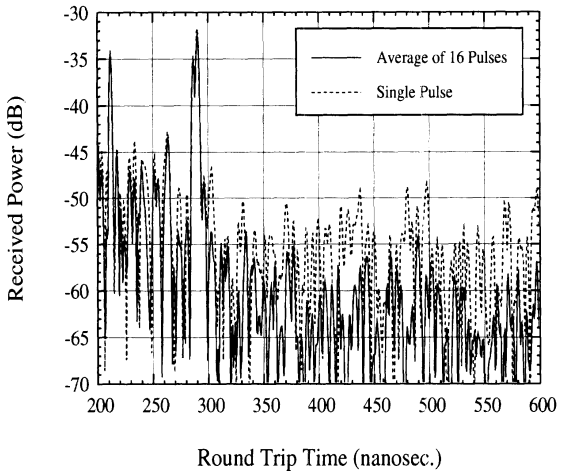

Figure 10: Comparison between the response of a single pulse and the coherently averaged response of 16 pulses. Coherent averaging provides about 6 dB improvement in the target signal-to-mean noise floor ratio.

a point target (trihedral) where it was shown that the SNR was improved by the averaging process as expected. It was also found that there was no significant difference between the two schemes, except that the frequency-domain approach is computationally more intensive when compared to the time-domain approach. We were able to achieve about 9 dB improvement in SNR by averaging the return from a small sphere over 8 consecutively transmitted pulses (SNR improvement using coherent averaging is proportional to $10log_{10}N$ with $N = 8$). In Fig. 10, the time-domain response of 16 coherently averaged returns using the time-domain scheme is compared with the response of a single pulse. In this case, coherent averaging of 16 pulses have resulted in about 6 dB improvement in the SNR instead of the expected 12 dB. This can be attributed to the presence of targets with strong radar returns located close to the radar (these returns are not shown in the figure). Since the dynamic range of the system is governed by the 50 dB dynamic range of the DO, the presence of strong targets in the signal path results in the "noise floor" being contaminated by the quantization errors of the DO, hence, reducing the effectiveness of coherent averaging in this case.

4. SYSTEM CALIBRATION AND VALIDATION

Characterization of measurement accuracy and precision are critical for any meaningful phenomenological radar measurement. Imperfections in the radar system components, such as antenna polarization contamination (coupling between the orthogonal polarization ports of the antenna) and channel imbalances (variations in magnitude and phase of the system transfer function for different ports of the receiver) can lead to serious errors in the measured scattering matrix. The role of a calibration procedure is then to remove the systematic errors from the measured target response. A number of calibration techniques have been reported in the literature, some were intended for coherent-on-receive radar systems [4, 9], while others were intended for coherent systems [10-14], such as the radar system proposed in this paper. In these calibration techniques, one or more calibration targets with known radar cross sections are measured, from which systematic errors are quantified and thus removed. The number of calibration targets needed and the complexity of a chosen calibration procedure depend mostly on the radar architecture and the required measurement accuracy. Since the MMW RF frontends considered in this paper possess high polarization isolation in their antenna assemblies (25 dB and 30 dB cross-polarization isolation for the 35-GHz and 95 GHz-RF frontends, respectively), the Isolated Antenna Calibration Technique (IACT) introduced by Sarabandi *et. al* [13] was used to calibrate the systems.

In the IACT technique, the antenna assembly is assumed distortionless, which is a good approximation for the new system, and only channel imbalances between the receiver ports need to be corrected for. As a result, calibration is accomplished through the measurement of a metallic sphere of known diameter (its radar cross section can be computed exactly) and any depolarizing target (unknown cross section). It is straightforward to show that channel imbalances in the system can be decomposed into time dependent quantities (amplifier gain, etc.) and time invariant quantities (waveguide loss, etc.). Both the metallic sphere and the depolarizing target need to be measured once indoors, from which time-invariant quantities can be determined. For subsequent calibrations, especially in outdoor settings, it can be shown that only a sphere measurement is needed for characterizing time-dependent distortions.

The validity of the IACT technique for calibrating the scattering matrices measured by the new system was examined. A 2-inch diameter sphere and a 20^o tilted dihedral were used as the calibration targets. A conducting cylinder with a diameter of 0.23 cm and a length of 3.665 cm was chosen as a test target. The cylinder was oriented at an angle of 43^o from vertical in a plane normal to the direction of incidence. Target orientation was facilitated by an elevation-over-azimuth positioner.The measured scattering matrix of the cylinder was compared with that computed using a method of moments (body of revolution) code. Considering the number of degrees of freedom in orienting the cylinder and radar platforms, excellent agreement was achieved between the theoretical and measured scattering matrix elements of the cylinder. This comparison is shown in Fig. 11 where maximum discrepancies of about 1.0 dB in magnitude and $\pm 10^o$ in phase were observed. Similar results were observed for the 95-GHz scatterometer. These measurements were repeated many times and consistent results were achieved.

To demonstrate the accuracy of the new ultra-fast wide-band radar system in the context of distributed target measurements, a dry smooth asphalt surface with an rms height s = 0.34 mm and correlation length l=4.2 mm was measured using both the new 35-GHz and 95-GHz systems. The same surface was measured two years earlier using a network analyzer-based polarimetric scatterometer operating at 95-GHz [15]. The two experiments were conducted from different platforms and by different individuals using different data acquisition, control, and processing software. In addition, calibration of the network analyzer-based system was performed following the technique developed by Nashashibi *et. al* [9], whereas the IACT calibration technique was used for the new system. In Fig. 12, the co- and cross-polarized backscattering coefficients of the asphalt surface from the two experiments are plotted as a function of the incidence angle θ (nadir looking is at θ= 0^o). Excellent agreement was observed between the two 95-GHz data sets indicating that the new system's performance (which is representative of the quality of its design, signal processing techniques, and calibration) in characterizing the radar response of clutter as well as point targets is comparable with that of currently available scatterometers.

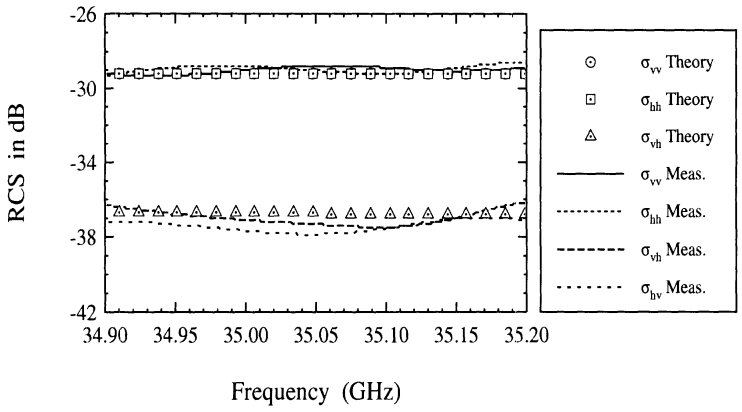

(a)

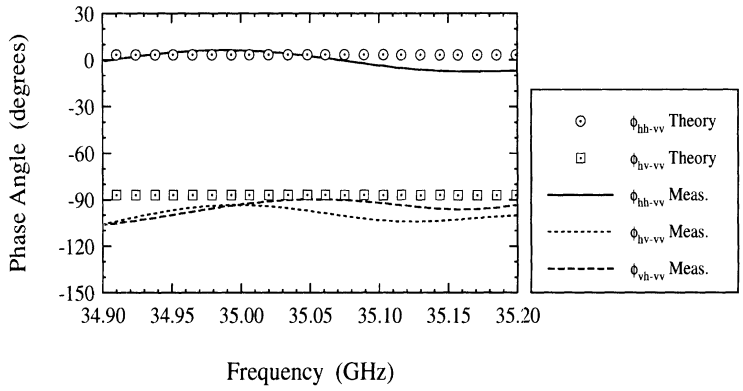

(b)

Figure 11: The magnitude (a) and phase difference (b) of the scattering matrix elements of a metallic cylinder (3.665 cm in length and 0.23 cm in diameter) oriented at 43^o from vertical.

5. EXAMPLE OF REMOTE SENSING STUDIES OF TERRAIN

The new radar system was operated in an imaging mode as part of an effort to characterize the polarimetric radar backscatter response of a corn field at near grazing incidence. Since our objective in this paper is to demonstrate the capabilities of the new system, only the attenuation rate incurred upon a wave propagating through the corn field will be discussed here. Full analysis of the polarimetric scattering properties of short vegetation at MMW frequencies will be the subject of a separate paper. Radar images of the corn field were acquired over a period extending from late July (plants were fully grown and green) to late October (plants were fully dry). The corn

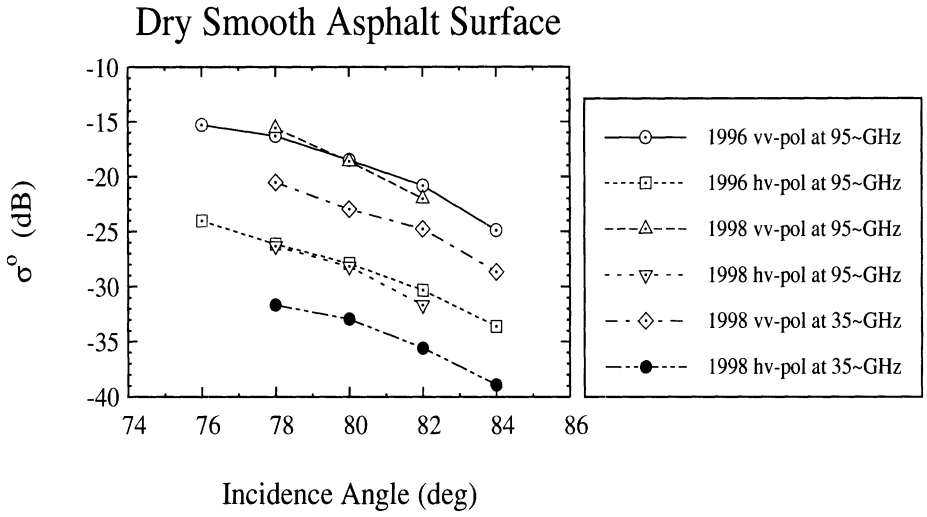

Figure 12: The backscattering coefficients of a dry smooth asphalt surface measured once in 1996 using a network analyzer-based scatterometer operating at 95 GHz, and measured one more time in 1998 using the new ultra-fast wide-band scatterometers at 35 GHz and 95 GHz. The rms height and correlation length of the asphalt surface were 0.34 mm and 4.2 mm respectively.

stalks were planted in rows with an average distance between rows of 95 cm. The average distance between any two adjacent plants within a row was 20 cm. During these measurements, the radar system was positioned at a fixed distance (16 m) away from the edge of the corn field and performed azimuthal scans perpendicular to the rows in the field. In each scan, between 50 and 80 statistically independent spatial samples were measured. An example of the radar image generated at 35-GHz using the new system is shown in Fig. 13. In this image, the 35-GHz radar signal was able to penetrate through the corn field and detect the periodicity characteristic of the corn-field structure. This pattern was also observed at 95-GHz, for corn plants under both dry and green conditions.

To determine the attenuation rate for this corn field for a given scan, an average radar return was calculated first by averaging the backscatter returns at every rangebin over all measured spatial samples in that scan. An example of the averaged return as a function of the round trip time is shown in Fig. 14 for the vv- and hh-polarized returns of a dry corn field measured at 95-GHz. It should be noted that since scanning was done perpendicular to the rows in the field, the process of averaging the samples did not destroy the periodicity in

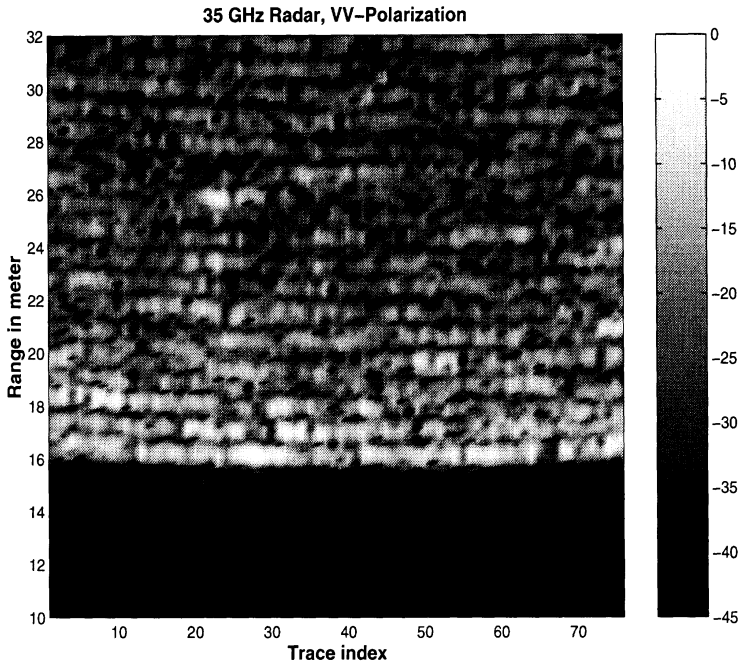

Figure 13: A vv-polarized near-grazing radar image of a corn field measured at 35 GHz. The normalized received power is plotted versus range in meter.

the averaged return. Since no physical anomalies were observed in the corn field, it can be safely assumed that the field is a statistically homogeneous random medium. In this case, the reduced return from any given row is the result of the round trip attenuation suffered by the radar signal as it propagated through the rows that were present between the radar and the row of interest. This attenuation can be attributed to both scattering and absorption in the corn plants. The ratio between the received powers of successive peaks can be used to compute the average round trip propagation loss per row in this corn field. Figure 15 demonstrates the trend in the average round trip propagation loss per row of the corn field during its life cycle at both 35 and 95-GHz (in this figure, m_g refers to the average gravimetric moisture content in the plants). The figure clearly demonstrates the impact of the plant moisture content on the penetrability of the corn field.

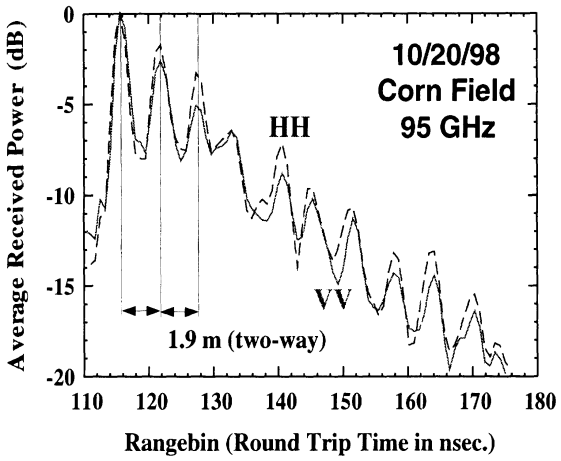

Figure 14: The average time-domain return from dry corn at 95 GHz.

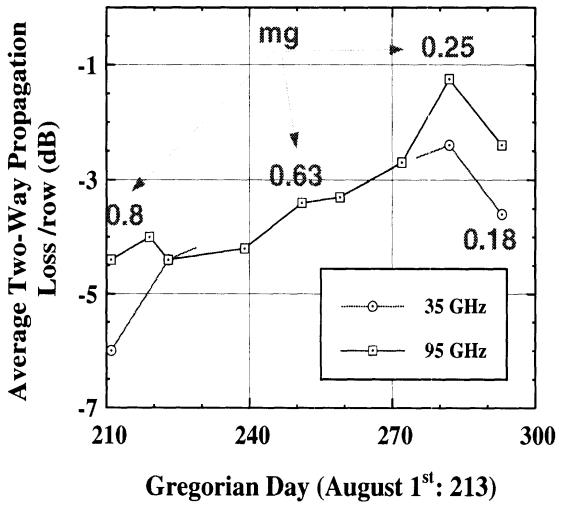

Figure 15: Two-way propagation loss per row in a corn field during its life cycle measured at both 35 and 95 GHz, as a function of, m_g, the average gravimetric moisture content in the plants. Increased plant moisture is correlated with increased propagation loss.

6. CONCLUSIONS

A pair of new MMW wide-band polarimetric instrumentation radars were developed at The University of Michigan for remote sensing applications. With the new system design, the scattering matrix of a target can be measured over a bandwidth of 500 MHz in as little as 2 μsec. The short data-acquisition time ensures correct characterization of the complex scattering matrix elements. Details of the system design were discussed along with data acquisition, signal processing, and external calibration techniques. The capability of the new system to properly characterize the backscattering coefficients of distributed targets was demonstrated. In addition, its ability in generating fully polarimetric radar images of one foot resolution was demonstrated. Sample images obtained from a corn field show periodicity in the corn row structure and were used to determine the average round trip propagation loss through the corn field as a function of plant moisture content at both 35 and 95 GHz.

ACKNOWLEDGMENT

The authors would like to thank Bruce Wallace, Ron Wellman, Eric Adler, and Marvin Conn of the Army Research Laboratory for their helpful suggestions during the initial phases of the radar design.

REFERENCES

[1] Huynen, J.R., "Measurement of target Scattering Matrix," *Proc. IEEE,* vol. 53, pp. 936-946, 1965.

[2] Ulaby, F.T. and C. Elachi *Radar Polarimetry for Geoscience Applications,* Artech House, Dedham MA, 1990.

[3] Ulaby, F.T., M.W. Whitt, and K. Sarabandi, "AVNA-based polarimetric scatterometers," IEEE AP magazine, vol. 32, 1990.

[4] Mead, J.B., "Polarimetric measurements of foliage and terrain at 225 GHz," Ph.D. dissertation ,University of Massachusetts, 1990.

[5] Wellman, R. J., J. Nemarich, H. Dropkin, D. R. Hutchins, J. L. Silvious, and D. A. Wikner, "Polarimetric Monopulse Radar Scattering Measurements of Targets at 95 GHz," *AGARD Conf. Proceed.*, vol. 501, pp. 30-1–30-13, Sept. 1991.

[6] DCP-1 Chirp Synthesizer, Sciteq Electronics, Inc. San Diego, California 92123.

[7] N. Levanon *Radar Principles,* John Wiley & Sons, New York NY, 1988.

[8] M. I. Skolnik Introduction to Radar Systems, McGraw-Hill, New York, NY, 1980.

[9] Nashashibi, A., K. Sarabandi, and F.T. Ulaby,"A Calibration Technique For Polarimetric Coherent-On-Receive Radar Systems," *IEEE Trans. Antennas and Propagat.*, vol. 43, no. 4, pp. 396-404, April 1995.

[10] Barnes, R.M., "Polarimetric calibration using in-scene reflectors," Rep. TT.65, MIT, Lincoln Laboratory, Lexington, MA, Sept. 1986.

[11] Whitt, M.W., F.T. Ulaby, P. Polatin, and V.V. Liepa, "A general polarimetric radar calibration technique," *IEEE Trans. Antennas Propagat.*, vol. 39, no. 1, pp. 62-67, Jan. 1991.

[12] Whitt, M.W. and F.T. Ulaby,"A polarimetric radar calibration technique with insensitivity to target orientation," *Radio Sci.*, vol. 25, no. 6, pp. 1137-1143, Nov.-Dec. 1990.

[13] Sarabandi, K., F.T. Ulaby, and M.A. Tassoudji, "Calibration of polarimetric radar systems with good polarization isolation", *IEEE Trans. Geosci. Remote Sensing*, vol. 28, no. 1, 1990.

[14] Sarabandi, K., and F.T. Ulaby, "A convenient technique for polarimetric calibration of radar systems", *IEEE Trans. Geosci. Remote Sensing*, vol. 28, No. 6, pp. 1022-1033, Nov. 1990.

[15] Sarabandi, K., E. S. Li, and A. Y. Nashashibi, "Modelling and Measurements of Scattering from Road Surfaces at Millimeter-Wave Frequencies," *IEEE Trans. Antennas and Propagat.*, Vol. 45, No. 11, pp. 1679-1688, Nov. 1997.